Evolution of Soft Zone in a Simulated 1.25Cr-0.5Mo Steel-Welded Joint During Post-weld Heat Treatment

YANG SHEN, ZHENGMAN GU, and CONG WANG

In the present study, the effect of post-weld heat treatment on the soft zone of 1.25Cr-0.5Mo steel welded joint has been systematically studied. Outstanding features of the soft zone, including grain size, number density of carbides, volume fraction of carbides, and hardness distribution, are quantitatively analyzed by means of scanning electron microscopy and a microhardness testing. Results show that ferrite grain growth, carbide coarsening, and alloying element segregation are main factors accounting for hardness variations.

https://doi.org/10.1007/s11661-021-06225-5
© The Minerals, Metals & Materials Society and ASM International 2021

1.25Cr-0.5Mo ferritic heat-resistant steel has been universally employed for fabricating heat exchangers and superheater tubes in thermal powering applications.[1] Such large-scale pressure vessel components normally require welding and post-weld heat treatment (PWHT) before being positioned into high-temperature service.[2,3] Up to now, a consensus has been formed that the location of short-term creep failure, commonly coined as soft zone, is identified in the fine-grained heat-affected zone (FGHAZ) or intercritical heat-affected zone (ICHAZ) of the welded joints, where hardness values are generally lower.[4–6] Consequently, it is of technical significance to identify the presence, investigate the formation mechanism, and profile possible microstructural and mechanical responses of the soft zone.

However, it is notable that most previous studies only focused on observing the microstructures of the soft zone in Cr-Mo steel weldments after creep tests, trying to clarify creep rupture mechanisms.[7,8] Sawada *et al*.[9] suggested that the multiaxiality of stress promoted *Z*-phase formation in the FGHAZ of E911 steel during creep, resulting in an abrupt decrease in hardness and a higher creep cavity density. Shrestha *et al*.[10] investigated creep rupture behavior of fusion-welded Grade 91 steel and discovered that the fracture point had the lowest hardness of 56 VHN. Laha *et al*.[11] reported that the pronounced hardness drop and creep fracture were observed in the ICHAZ of the welded joints of a 2.25Cr-1Mo steel after creep testing, which might be attributed to the absence or less abundance of the fine acicular Mo_2C precipitates in the ICHAZ.

Moreover, microstructural features and formation mechanisms of the soft zone are not well understood during welding and PWHT procedures. Wang *et al*.[6] concluded that the initial soft zone was identified to be formed at the as-welded state by using microhardness profiling and microstructural verification. Heterogeneous structure observed in the soft zone, consisting of Cr-rich re-austenitized prior austenite grains and fine Cr-depleted, tempered martensite grains, could be directly responsible for the hardness reduction. Albert *et al*.[12] demonstrated that the soft zone imparted by the migration of carbon in a dissimilar welded joints between 9Cr-lMo and 2.25Cr-1Mo steels could be observed after applying PWHT. It should be pointed out that tracking the soft zone structure back to the initial as-welded and PWHT states may likely provide an insight into state-of-the-art understanding of the formation mechanisms and microstructural evolution of the soft zone, which has been largely ignored.

Therefore, from the above point of view, the present work aims to determine the exact position of the soft zone in 1.25Cr-0.5Mo steel after notable checking points, such as welding and PWHT, and systematically investigate microstructural evolution and mechanical performance. In addition, an in-depth understanding of the mechanism of hardness variation in the soft zone under varying PWHT schemes is presented, which might offer an optimized PWHT scheme for pressure vessel industry and contribute to comprehend premature failure mechanisms of the final products.

1.25Cr-0.5Mo steel (ASTM A378 Grade 11 Class 2) was used as the base material, and corresponding chemical composition is shown in Table I.

YANG SHEN and ZHENGMAN GU are with the School of Metallurgy, Northeastern University, Shenyang 110819, P.R. China. CONG WANG is with the School of Metallurgy, Northeastern University and also with the State Key Laboratory of Rolling and Automation, Northeastern University, Shenyang 110819, China Contact e-mail: wangc@smm.neu.edu.cn

Manuscript submitted December 9, 2020, accepted February 25, 2021.

Article published online March 21, 2021

Detailed heating and cooling procedures for heat treatment and welding are presented in Figure 1. The as-received steel plate with dimensions of 140 mm in width (rolling direction), 410 mm in length, and 110 mm in thickness was held at 1203 K above Ac_3 (1085 K) for 220 minutes, quenched into water, tempered at 1003 K below Ac_1 (1036 K) for 330 minutes, and air cooled, which is referred to as the QT state. To simulate welding, samples with a size of 11 × 11 × 80 mm were cut from the position which was near the 1/2 thickness of the QT state steel plate for welding simulation on a thermal simulation tester (Gleeble 3500, Dynamic system INC.). The peak welding temperature was 1673 K with a holding time of 1 second, and the cooling time from 1073 K to 773 K ($t_{8/5}$) was estimated to be 7.07 seconds, which was designed to simulate shielded metal arc welding with 12 kJ/cm heat input.[13] Thermal cycle was described by employing the Rykalin-3D heat transfer model. The farther away from the center of the heat source, the lower the peak temperature is. Therefore, graded microstructure can be obtained as the direct result of cascaded temperature distribution. For convenience, samples subjected to welding simulation without PWHT are designated as the as-welded (AW) state. Afterwards, AW state samples were sealed into a quartz tube, evacuated, and argon filled to prevent oxidation during PWHT. The tube was placed into a pit-type crucible furnace (VF-1200X, China), heated from 673 K to 963 K at a rate of 55 K/h, held for desired durations (6 hours, 48 hours, and 480 hours), cooled to 673 K at a rate of 55 K/h, and then air cooled to room temperature. These sample are labeled as P6, P48, and P480, respectively.

Table I. Chemical Composition of 1.25Cr-0.5Mo Steel (Weight Percent)

C	Si	Mn	Cu	Ni	Cr	Mo	P	S
0.13	0.52	0.54	0.02	0.18	1.42	0.63	0.006	0.0011

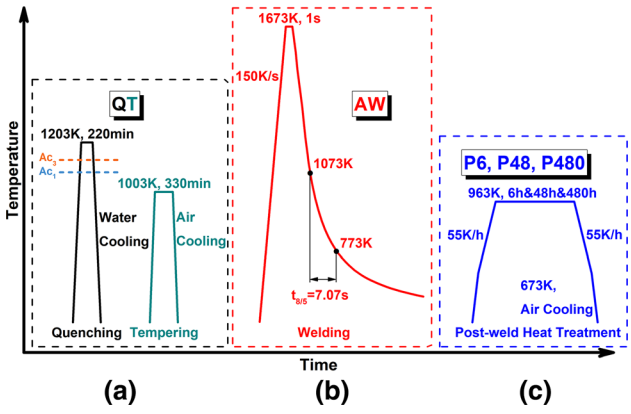

Fig. 1—Thermal cycles of (*a*) quenching and tempering, (*b*) welding, and (*c*) post-weld heat treatment.

For microhardness characterization, cross-sectional specimens were cut from AW state and PWHT state samples. These specimens were mounted, ground, polished, and etched with 4 pct (Percent) nital for 10 seconds (s) by using standard metallographic procedures. Vickers hardness across the cross section of the etched specimens was measured with a load of 0.2 kgf, a dwell time of 12 seconds, and an indentation spacing of 200 μm with the straight lines separated by a distance of 1 mm by using a microhardness tester (HXD-1000TMC/LCD, China). Five lines were obtained to ensure repeatability. Microstructures of the base metal (BM) and HAZ were characterized using a field-emission scanning electron microscope (FESEM, MAIA3 XMH, TESCAN, CZ). The average grain size of different state specimens was measured from SEM images by the intercept method (ASTM E12) using the ImageJ software.[14] Precipitate morphology was examined by an FE transmission electron microscope (TEM, Tecnai F20, FEI, U.S.A.). Elemental distribution was revealed by an FE electro-probe microanalyzer (EPMA, JXA-8530F, JEOL, Japan) combined with a wavelength-dispersive X-ray spectroscope (WDS). More detailed descriptions of TEM and EPMA specimen preparations are presented elsewhere.[15]

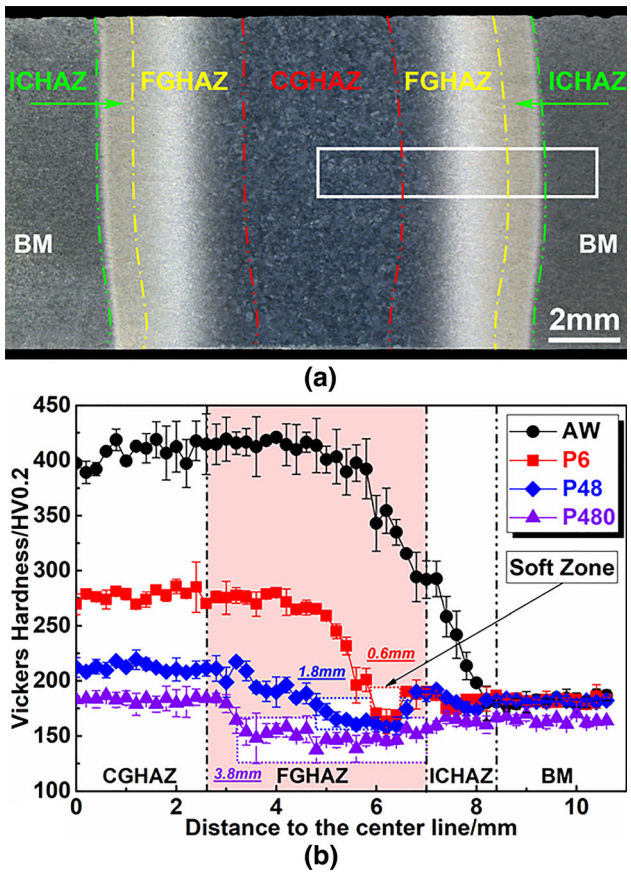

Fig. 2—(*a*) Macrograph of the entire HAZ of 1.25Cr-0.5Mo steel (The region marked by white rectangle is used for hardness test); (*b*) hardness distributions across the entire HAZ at the AW and PWHT states. (Three white shadows with red, blue, and violet dash lines represent the soft zones after PWHT at 963 K for 6, 48, and 480 h, respectively) (Color figure online).

Figure 2(a) presents the etched macrograph of the entire HAZ of 1.25Cr-0.5Mo steel, which clearly consists of three different zones, including coarse-grained heat-affected zone (CGHAZ), FGHAZ, and ICHAZ. Microhardness line scanning was conducted at the mid-thickness across the entire HAZ (marked by the white rectangle in Figure 2(a)) to show the hardness distribution and identify the location of the soft zone. Figure 2(b) shows the average microhardness profile across the entire HAZ at both the AW and PWHT (963 K for different durations) states. Statistical results of the HAZ hardness values under four thermal states are further compared in Table II.

As the bainitic structure is inside coarse prior austenite grains (PAGs),[16] the CGHAZ of the AW shows the highest hardness value (above 400 HV0.2). Moving along the center line, the hardness value cascades from 385.9 HV0.2 (FGHAZ) to 223.6 HV0.2 (ICHAZ), and to 182.6 HV0.2 (BM) as a result of lowered peak temperature and reduced soaking time.

Following PWHT, the hardness value of the HAZ demonstrates an ever-decreasing trend. The CGHAZ hardness sharply decreases from 407.0 HV0.2 (AW) to 277.1 HV0.2 (P6), 212.0 HV0.2 (P48), and 182.8 HV0.2 (P480), which indicates that an even greater tempering effect on lowering the hardness can be obtained *via* PWHT for a sufficiently long time. In the case of the FGHAZ, a hardness dip (167.6 HV0.2 in P6), which is lower than BM, occurs in the FGHAZ close to the ICHAZ after PWHT holding for 6 hours, indicated by the white shadow with red dash lines in Figure 2(b). This hardness dip has been identified as the soft zone, as illustrated by previous studies.[4] With the increase of holding time, as displayed by the white shadows with blue and violet dash lines from Figure 2(b), it can be seen that the hardness value of the soft zone gradually decreases from 164.2 HV0.2 (P48) to 149.5 HV0.2 (P480). In addition, it is observed that the widths of the soft zone of P48 and P480 are considerably wider than those of P6, increasing from 0.6 to 1.8 mm and to 3.8 mm. It can be found that the soft zone first appears in the FGHAZ close to the ICHAZ, then gradually widened, and occupied almost the entire FGHAZ after prolonged PWHT. The hardness of the ICHAZ on the right side maintains between 160 HV0.2 and 180 HV 0.2 without significant reduction, which is consistent with changes in the BM.

Simultaneously, it is seen that the hardness difference between the sub-zones of the HAZ continuously decreases. Hardness variations within the HAZ are below 30 HV0.2 after PWHT at 963 K for 480 hours. It is implied that a homogenized HAZ with uniform hardness values can be obtained by long-term PWHT.[7]

Figure 3(a) shows the typical microstructure of 1.25Cr-0.5Mo steel of the QT state. It has a characteristic tempered troostite structure, which is mainly composed of lath ferrite, with sizable amount of fine granular carbides evenly distributed inside the grains. The average grain size of the QT state is 2.4 μm. Figure 3(b) shows the TEM image of the QT state, where rod-shaped and globular-shaped carbides are evenly distributed, with a size ranging from 100 to 200 nm. A selected area electron diffraction pattern, represented in the inset of Figure 3(b), indicates that the Cr-rich carbide is M_7C_3-type carbide with hexagonal structure, which is consistent with a previous study.[15]

Figures 3(c) through (f) exhibit quintessential micrographs of the soft zones at four different thermal states. As shown in Figure 3(c), an equiaxed PAGs structure with an average size of 8.6 μm is observed in the FGHAZ close to the ICHAZ of the AW state. Bainites and undissolved carbides are the main substructures within the PAGs. Unlike the PAGs structure in Figure 3(c), the soft zone after PWHT at 963 K for 6 hours (P6) in Figure 3(d) shows a structure consisting of blocky ferrites and fine granular carbides evenly distributed inside the grains, which implies that PWHT has significantly altered the microstructure of the soft zone. As shown in Figure 2(b), it is believed that the initial softening from the AW to the P6 state appears to be related to the transition from a bainitic ferrite to a blocky ferrite microstructure where the reduction in dislocation density may be the dominant softening mechanism.[17,18] Furthermore, after 48 hours of PWHT, the microstructure of the soft zone carries a mixture of coarse blocky ferrites and carbides, as shown in Figure 3(e). After 480 hours of PWHT, the microstructure of the corresponding soft zone has evolved to equiaxed ferrites and coarse globular carbides, as shown in Figure 3(f).

Average grain sizes of ferrites at different PWHT states are shown in Figure 4(a). It can be seen that with the PWHT holding time mounting, the average grain size increases from 4.9 μm (P6) to 10.5 μm (P48) and to 14.6 μm (P480), which indicates appreciable ferrite grain growth.[19] Grain refining is commonly known to enhance strength and hardness of polycrystalline materials. In particular, it is widely accepted that the yield strength of a metallic material as a function of grain size can be well described by the empirical Hall–Petch Eq. [1],[20–22]:

Table II. Average Vickers Hardness Values of the Sub-zones of the HAZ at Various Thermal States (HV0.2)

Thermal State	CGHAZ	FGHAZ	ICHAZ	BM
AW	407.0 ± 10.0	385.9 ± 42.7	223.6 ± 42.4	182.6 ± 3.1
P6	277.1 ± 5.4	236.5 ± 43.2	181.7 ± 5.3	182.5 ± 2.1
P48	212.0 ± 3.5	182.5 ± 18.1	181.5 ± 6.2	181.6 ± 1.8
P480	182.8 ± 2.4	152.1 ± 11.2	163.4 ± 3.0	164.7 ± 3.3

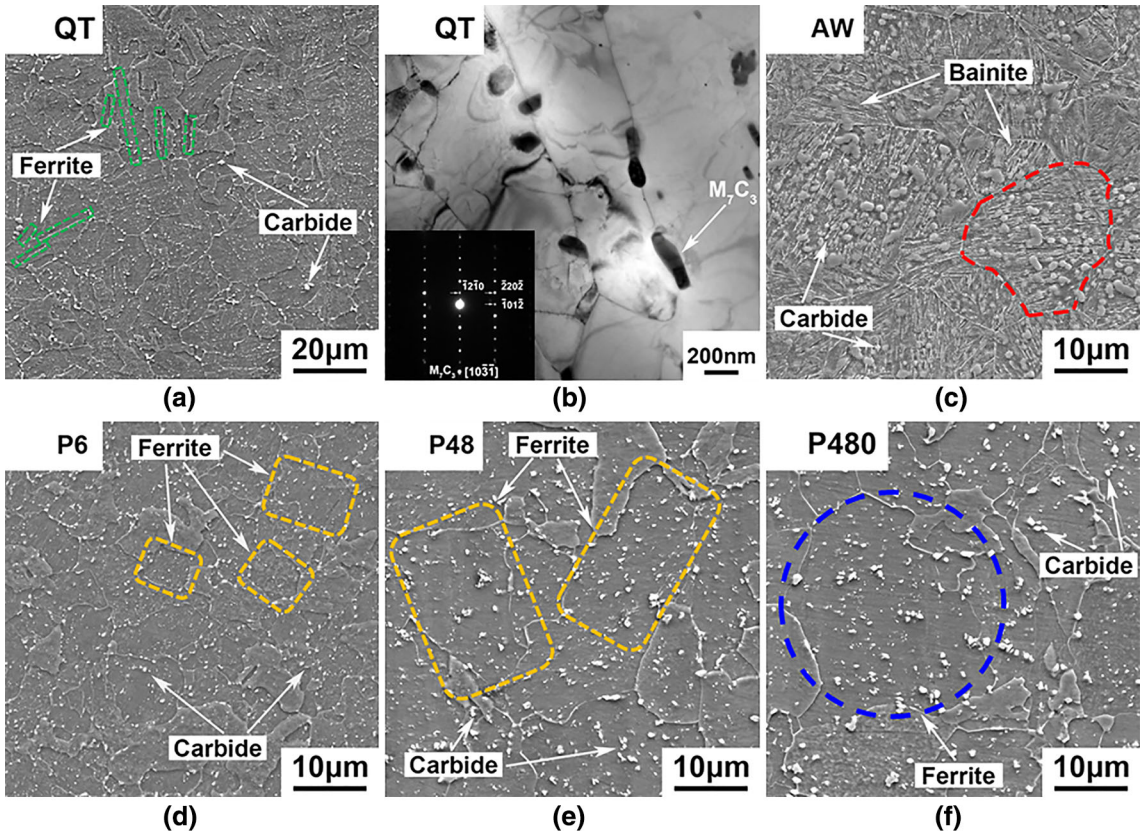

Fig. 3—Typical microstructural features of 1.25Cr-0.5Mo steel observed at the QT state: (*a*) SEM micrograph and (*b*) TEM micrograph; SEM micrographs showing the microstructure of the soft zone at (*c*) AW, (*d*) P6, (*e*) P48, and (*f*) P480 states. (Green, red, yellow, and blue dash lines represent lath ferrites, prior austenite grain boundaries, blocky ferrites, and equiaxed ferrites, respectively) (Color figure online).

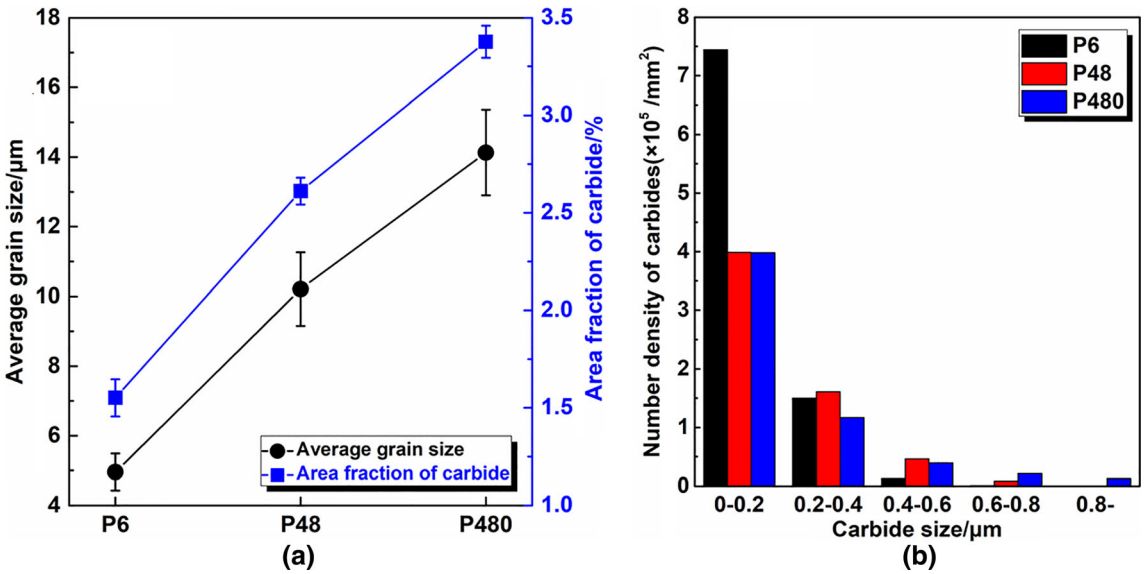

Fig. 4—(*a*) Average grain sizes of ferrites and area fraction of carbides as a function of PWHT holding time; (*b*) number density and size distribution of carbides at different thermal states.

$$\sigma_y = \sigma_0 + kD^{-1/2}, \qquad [1]$$

where σ_y is yield strength, σ_0 (100 MPa) and k (600 MPa $\mu m^{1/2}$) are constant, D is grain size, and the

relationship between the hardness and yield strength also approximately follows the Eq. [2] as below:[23]

$$H \approx 3\sigma_y \quad [2]$$

where H is the Vickers hardness. According to Eqs. [1] and [2], with the increase of grain size, the value of hardness will decrease to H_{P6} = 1113.2 MPa, H_{P48} = 855.5 MPa, and H_{P480} = 771.1 MPa, respectively. However, Vickers hardness values of P6, P48, and P480 states measured from the experiment are not strictly followed by the linear relationship between H and $D^{-1/2}$. Thus, in the present work, it can be considered that ferrite grain growth may merely constitute part of the reasons for the hardness reduction.

Concurrently, as shown in Figure 4(a), the area fraction of carbides is 1.6 pct (P6), 2.6 pct (P48), and 3.4 pct (P480), respectively. It is observed that the area fraction of P480 is twice that of P6. Moreover, the evolution of number density and size distribution of carbides at P6, P48, and P480 states is shown in Figure 4(b). The number density of carbides in P6 specimen is $9.08 \times 10^5/\text{mm}^2$, and their average size is 0.35 μm. After 48 hours of holding time, the number density of carbides decreases to $6.14 \times 10^5/\text{mm}^2$ and the size distribution of carbides has undergone significant change. The number density of carbides less than 0.2 μm decreases, while that of large-size carbides ranging from 0.4 to 0.6 μm increases significantly. With the increase of holding time, the number density and size distribution of carbides in P480 undergo appreciable change. The number density and average size turn into $5.89 \times 10^5/\text{mm}^2$ and 0.49 μm, respectively. It can be seen that, comparing with P6 and P48, the number of carbides larger than 0.6 μm in P480 increases substantially. To a large extent, PWHT is equivalent to high-temperature tempering treatment.[24] As the PWHT holding time increases, a large number of fine carbides aggregate and coarsen in the grain, which is considered to be responsible for the decrease of number density and the increase of carbide size. Based on the measured particle sizes and particle number densities, the volume fraction of particle can be expressed by Eq. [3] as below:[25]

$$f = \frac{\pi^3}{24} \cdot \bar{d}_A^2 \cdot N_A, \quad [3]$$

where f is the volume fraction of precipitates, d_A is the diameter of precipitates, and N_A is the number of precipitates sections per unit area. According to Eq. [3], with the increase of holding time, the volume fraction of precipitates increases from 2.36 pct (P6), to 3.92 pct (P48), and eventually to 5.49 pct (P480).

In addition to the effect of grain size on hardness, coarsened carbides may lead to depressed precipitation strengthening, which is also considered to be detrimental to hardness. Precipitation strengthening in steels is usually estimated by the Orowan–Ashby Eq. [4]:[26,27]

$$\sigma_y = \frac{K}{d} f^{1/2} ln \frac{d}{b}, \quad [4]$$

where K is a constant (5.9 N/m), b is the burgers vector (0.246 nm), and d and f are the average diameter and volume fraction of precipitates. According to Eqs. [2] and [4], the calculation shows that the decrease in hardness during PWHT can be explained by a reduction of precipitation strengthening due to the coarsening of carbides. Thus, during subsequent PWHT, *i.e.*, from P6 to P480, ferrite grain growth and carbide coarsening are observed. Both aspects may lead to a combined effect for hardness decrease and widening of the soft zone.

Moreover, the distributions of the main alloying elements, such as C, Cr, and Mo, in the soft zone of AW, P6, P48, and P480 states have been documented by EPMA-WDS in Figure 5. Backscattered electron (BSE) images of the AW and PWHT states are observed in Figures 5(a), (e), (i), and (m). Figures 5(b) through (d) show that distributions of C, Cr, and Mo are essentially uniform at the AW state, with a few high-intensity spots of Cr being identified as undissolved Cr-rich carbides. After 6 hours of PWHT, bainitic features gradually disappear and blocky ferrites are formed. Certain carbides with high C, Cr, and Mo contents may form along grain boundaries, as shown in Figures 5(f) through (h). As the PWHT holding time increased to 48 hours and 480 hours, more globular carbides with higher concentrations of C, Cr, and Mo appear to significantly populate and aggregate inside the grains, as demonstrated in Figures 5(j) through (l) and Figures 5(n) through (p), respectively. Combining the results of EPMA and calculated volume fraction of precipitates, it is postulated that solid solution strengthening is decreasing as PWTH prolongs. Since solid solution strengthening is one of the main strengthening mechanisms for Cr-Mo steel,[28] as PWHT holding time increases, carbides may likely precipitate and coarsen, and carbon in the matrix will be depleted, which will lead to appreciable hardness reduction.

Figure 6 provides a schematic illustration of microstructural evolution in the soft zones based on the above analyses after different thermal states. As shown in Figure 6(a), the original microstructure of the QT state consists of ferrite, with a large number of granular carbides evenly distributed inside the grains. During welding, as the FGHAZ is exposed to a peak temperature just above Ac_3 and a short soaking time, small carbides will completely dissolve into the austenite in the FGHAZ, while large carbides are partially dissolved, which may be present in the bainite matrix in Figure 6(b). When the welded joints are subject to PWHT, supersaturated carbon in bainite will assist the nucleation and growth of carbides. After PWHT at 963 K for 6 hours, blocky ferrites with fine granular carbides evenly distributed inside the grains are observed in Figure 6(c). With the PWHT holding time prolonged from 6 hours to 480 hours, the average grain size of ferrites increases from 4.9 to 14.6 μm, as fine blocky ferrites morph into equiaxed ferrites. More carbides are precipitated and aggregated inside the grains, and exhibit considerable coarsening and spheroidization. Dixit *et al.*[29] and Yang *et al.*[30] showed that tempering time played an important role in the evolution of microstructure and the associated

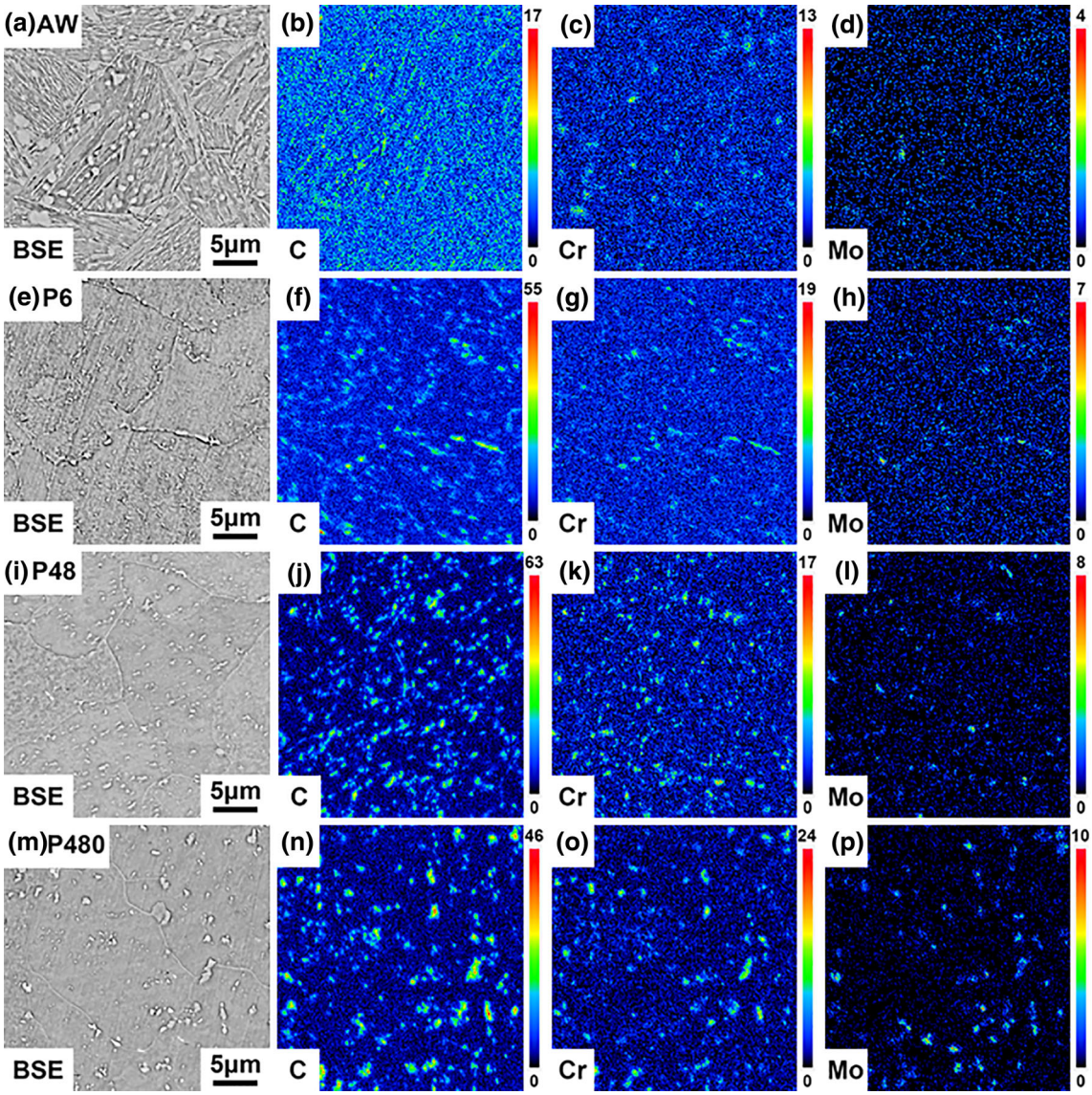

Fig. 5—EPMA results of C, Cr, and Mo for precipitates in the soft zone at (*a*) through (*d*) AW, (*e*) through (*h*) P6, (*i*) through (*l*) P48, and (*m*) through (*p*) P480 states.

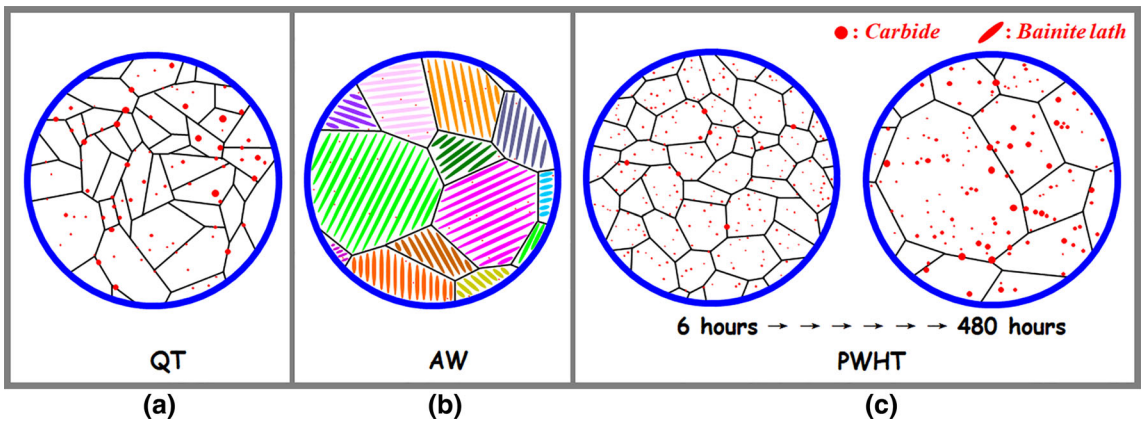

Fig. 6—Schematic illustration showing microstructural evolution in the soft zone at (*a*) QT, (*b*) AW, and (*c*) PWHT states.

changes in mechanical performance. Long-term service at high temperature may cause a significant growth of grains and coarsening of carbides. As a result, prolonged PWHT may promote sustained grain growth, continuous carbide coarsening, and depressed solid solution strengthening, which may constitute the main factors contributing to the decrease in hardness values and account for the evolution of the soft zone after prolonged PWHT.

In this work, microstructural features and mechanical responses of the soft zone in a simulated 1.25Cr-0.5Mo steel welded joint have been investigated, under continuous thermal histories, at the AW-ed and various PWHT-ed states. The main causes for the variation of the soft zone were proposed after extensive microscopic analysis. The conclusions are summarized as follows:

1. The soft zone could be accurately positioned in the region of the FGHAZ adjacent to the ICHAZ after PWHT. With the increase of PWHT holding time, the width of the soft zone increases from 0.6 mm (P6) to 1.8 mm (P48) and to 3.8 mm (P480). Concurrently, the hardness value of the soft zone decreases from 167.6 HV0.2 (P6) to 164.2 HV0.2 (P48) and to 149.5 HV0.2 (P480).
2. The microstructure of the soft zone is primarily composed of ferrite and carbides. As the PWHT holding time is mounting, the average grain size of ferrite in P6, P48, and P480 increases from 4.9 to 10.5 μm and to 14.6 μm, the number densities of carbides are 9.08×10^5, 6.14×10^5, and 5.89×10^5 /mm^2, and their average size are 0.35, 0.38, and 0.49 μm, respectively.
3. The combined effects of grain growth, carbide coarsening, and alloying elements segregation during PWHT will lead to a decrease in hardness, which is believed to lower creep strength and eventually fail with short-term service.

ACKNOWLEDGMENTS

The authors wish to thank the financial supports from the National Natural Science Foundation of China (Grant Nos. U20A20277, 51861130361, 51861145312, 51850410522, 52050410341, and 52011530180), Newton Advanced Fellowship by the Royal Society (Grant No. RP12G0414), Royal Academy of Engineering (Grant No. TSPC1070), Special Fund for Key Program of Science and Technology of Liaoning Province (Grant No. 2019JH1/10100014), The Fundamental Research Fund for Central Universities (Grant No. N2025025), Regional Innovation Joint Fund of Liaoning Province (Grant No. 2020-YKLH-39), Natural Science Foundation of Liaoning (Grant No. 2019KF0502), and Xingliao Talents Program (Grant Nos. XLYC1807024 and XLYC1802024). The authors also greatly appreciate the support from Jiangyin Xingcheng Special Steel Works Co., Ltd.

REFERENCES

1. M.Y. Kim, M.G. Jo, J.Y. Suh, W.S. Jung, and J.H. Shim: *Mater. Charact.*, 2020, vol. 163, art. no. 110314, https://doi.org/10.1016/j.matchar.2020.110314.
2. B. Silwal, L. Li, A. Deceuster, and B. Griffiths: *Weld. J.*, 2013, vol. 92, pp. 80s–7s.
3. P. Dong, S. Song, and J. Zhang: *Int. J. Press. Vessels Pip.*, 2014, vol. 122, pp. 6–14.
4. S.A. David, J.A. Siefert, and Z. Feng: *Sci. Technol. Weld. Joining*, 2013, vol. 18, pp. 631–51.
5. Y. Liu, S. Tsukamoto, T. Shirane, and F. Abe: *Metall. Mater. Trans. A*, 2013, vol. 44A, pp. 4626–33.
6. Y. Wang, R. Kannan, and L. Li: *Metall. Mater. Trans. A*, 2018, vol. 49A, pp. 1264–75.
7. Y. Wang, L. Li, and R. Kannan: *Mater. Sci. Eng. A*, 2018, vol. 714, pp. 1–13.
8. C. Pandey, M.M. Mahapatra, P. Kumar, S. Kumar, and S. Sirohi: *J. Mater. Process. Technol.*, 2019, vol. 266, pp. 140–54.
9. K. Sawada, M. Bauer, F. Kauffmann, P. Mayr, and A. Klenk: *Mater. Sci. Eng. A*, 2010, vol. 527, pp. 1417–26.
10. T. Shrestha, M. Basirat, S. Alsagabi, A. Sittiho, I. Charit, and G.P. Potirniche: *Mater. Sci. Eng. A*, 2016, vol. 69, pp. 75–86.
11. K. Laha, K.S. Chandravathi, K. Bhanu Sankara Rao, S.L. Mannan, and D.H. Sastry: *Metall. Mater. Trans. A*, 2001, vol. 32A, pp. 115–24.
12. S.K. Albert, T.P.S. Gill, A.K. Tyagi, S.L. Mannan, S.D. Kulkarni, and P. Rodriguez: *Weld. J.*, 1997, vol. 76, pp. 135s–142s.
13. V.N. Lazić, A.S. Sedmak, M.M. Živković, S.M. Aleksandrović, R.D. Čukić, R.D. Jovičić, and I.B. Ivanović: *Therm. Sci.*, 2010, vol. 14, pp. 235–46.
14. C.A. Schneider, W.S. Rasband, and K.W. Eliceiri: *Nat. Methods*, 2012, vol. 9, pp. 671–75.
15. Y. Shen, H. Matsuura, and C. Wang: *Metall. Mater. Trans. A*, 2018, vol. 49A, pp. 4413–18.
16. Y. Shen, J. Leng, and C. Wang: *J. Mater. Sci. Technol.*, 2019, vol. 35, pp. 1747–52.
17. E.I. Galindo-Nava and P.E.J. Rivera-Díaz-Del-Castillo: *Scripta Mater.*, 2016, vol. 110, pp. 96–100.
18. S.H. He, B.B. He, K.Y. Zhu, and M.X. Huang: *Acta Mater.*, 2018, vol. 149, pp. 46–56.
19. C. Yue, L. Zhang, S. Liao, and H. Gao: *J. Mater. Eng. Perform.*, 2010, vol. 19, pp. 112–15.
20. E.O. Hall: *Proc. Phys. Soc. B*, 1951, vol. 64, pp. 747–53.
21. N.J. Petch: *J. Iron Steel Inst.*, 1953, vol. 174, pp. 25–28.
22. Y. Tanaka, S. Takaki, T. Tsuchiyama, and R. Uemori: *ISIJ Int.*, 2018, vol. 58, pp. 1927–33.
23. P. Zhang, S.X. Li, and Z.F. Zhang: *Mater. Sci. Eng. A*, 2011, vol. 529, pp. 62–73.
24. Q. Gao, X. Di, Y. Liu, and Z. Yan: *Int. J. Press. Vessels Pip.*, 2012, vol. 93, pp. 69–74.
25. K. Sakata and H. Suito: *Metall. Mater. Trans. B*, 1999, vol. 30B, pp. 1053–63.
26. Y. Funakawa, T. Shiozaki, K. Tomita, T. Yamamoto, and E. Maeda: *ISIJ Int.*, 2004, vol. 44, pp. 1945–51.
27. M.P. Phaniraj, Y.M. Shin, W.S. Jung, M.H. Kim, and I.S. Choi: *Nano Converg.*, 2017, vol. 4, pp. 1–8.
28. W. Wei, Z. Wengui, and Q. Jinbo: *Steel Res. Int.*, 2013, vol. 84, pp. 178–83.
29. S. Dixit, V. Chaudhari, and D.M. Kulkarni: *J. Mater. Process. Technol.*, 2020, vol. 276, p. 116419.
30. Y. Yang, Y. Chen, K. Sridharan, and T.R. Allen: *Metall. Mater. Trans. A*, 2010, vol. 41A, pp. 1441–47.

Publisher's Note Springer Nature remains neutral with regard to jurisdictional claims in published maps and institutional affiliations.